Metallophysics and Advanced Technologies
Металофіз. новітні технол.
Metallofiz. Noveishie Tekhnol.
2022, vol. 44, No. 3, pp. 393–418
https://doi.org/10.15407/mfint.44.03.0393
Reprints available directly from the publisher

PHYSICS OF STRENGTH AND PLASTICITY

PACS numbers: 42.62.Cf, 81.05.Bx, 81.20.Ev, 81.20.Vj, 81.40.Gh

Ensuring Strength of the Seam of Thermal Protective Structures from Thin-Sheet Nickel Alloys Obtained by Laser Vacuum Welding

Walid Alnusirat, Alexandr Salenko[*], Sergiy Shlyk[**], Irina Gusarova[***], Petro Loboda[*], Iryna Trosnikova[*], and Iurii Bogomol[*]

Al-Balqa Applied University Al-Salt,
P.O. Box, 19117 Al-Salt, Jordan
[*]*National Technical University of Ukraine*
'Igor Sikorsky Kyiv Polytechnic Institute',
37 Peremohy Ave.,
03056 Kyiv, Ukraine
[**]*Kremenchuk Mykhailo Ostrohradskyi National University,*
20 Pershotravneva Str.,
UA-39600 Kremenchuk, Ukraine
[***]*Yuzhnoye Design Office,*
3 Kryvorizka Str.,
UA-49008 Dnipro, Ukraine

The results of studying the laser vacuum welding of the elements of heat-shielding structures made by dispersion-hardened alloys Ni–20Cr–6Al–Ti–Y_2O_3 of increased strength are presented. Also, the designs of the heat-insulating elements which are of cellular (honeycomb) structure consisting of two plates with thickness from 0.1 to 0.14 mm with fillers inside are considered. It is shown that the shallow thickness of the plates and the complexity of the design significantly complicate the possibility to firmly connect these elements and do not allow to use the known methods like diffusion welding or vacuum soldering. It is concluded that laser welding providing satisfactory structural strength and reliability can be an alternative to known methods. Local heating at certain points prevents deformation of the parts to be joined

Corresponding author: Iryna Trosnikova, Walid Alnusirat
E-mail: itrosnikova@gmail.com, alnusirat_w@protonmail.com

Citation: Walid Alnusirat, Alexandr Salenko, Sergiy Shlyk, Irina Gusarova, Petro Loboda, Iryna Trosnikova, and Iurii Bogomol, Ensuring Strength of the Seam of Thermal Protective Structures from Thin-Sheet Nickel Alloys Obtained by Laser Vacuum Welding, *Metallofiz. Noveishie Tekhnol.*, **44**, No. 3: 393–418 (2022).
DOI: 10.15407/mfint.44.03.0393

during the welding process. The use of a pulsed Nd:YAG laser with a power of 400–500 W operating in the frequency range of 50–200 Hz allows welding with and without filler metal. It has been established that the use of filler metal has practically no effect on the mechanical properties of the welded joint, however, it significantly reduces the melt zone and increases the density of the welded joint. Based on the obtained results, it is concluded that an increase of the joint strength is achieved due to the high purity of the vacuum chamber, low vacuum (less than 10^{-2} Pa), and optimization of the welding process. It has been proved that the use of laser welding in vacuum when assembling elements of heat-shielding structures makes it possible to obtain a stronger and denser seam compared to known methods.

Key words: laser vacuum welding, strength of a welded joint, dispersion-hardened alloys, heat-shielding structures.

У роботі наведено результати дослідження лазерного вакуумного зварювання елементів теплозахисних конструкцій, виготовлених з дисперсійно-загартованих стопів підвищеної міцності Ni–20Cr–6Al–Ti–Y_2O_3. Також розглянуто конструкцію теплоізоляційних елементів, які мають комірчасту (стільникову) структуру, що складається з двох плит товщиною від 0,1 до 0,14 мм з наповнювачами всередині. Показано, що невелика товщина пластин і складність конструкції істотно ускладнюють можливість міцного з'єднання цих елементів і не дозволяють використовувати відомі методи, такі як дифузійне зварювання або вакуумне лютування. Встановлено, що альтернативою відомим методам може бути лазерне зварювання, що забезпечує задовільну міцність і надійність конструкції. Локальний нагрів у певних точках запобігає деформації деталей, що з'єднують у процесі зварювання. Використання імпульсного Nd:YAG-лазера потужністю 400–500 Вт, що працює у діапазоні частот 50–200 Гц, дозволяє проводити зварювання як з металом присадкою, так і без нього. Встановлено, що використання металу присадки практично не впливає на механічні властивості зварного з'єднання, однак значно зменшує зону розтопу та підвищує щільність зварного з'єднання. На основі одержаних результатів виявлено, що підвищення міцності з'єднання досягають за рахунок високої чистоти вакуумної камери, низького вакууму (менше 10^{-2} Па) та оптимізації процесу зварювання. Доведено, що використання лазерного зварювання у вакуумі для складання елементів теплозахисних конструкцій дає можливість одержати міцніший і щільніший шов порівняно з відомими способами.

Ключові слова: лазерне вакуумне зварювання, міцність зварного з'єднання, дисперсійно-загартовані стопи, теплозахисні конструкції.

(Received October 27, 2021; in final version, December 15, 2021)

1. INTRODUCTION

The designs of heat-shielding elements of reusable spacecraft with an external metal panel are being actively developed by leading experts from many countries [1, 2]. In fact, that the most effective thermal

protection consists of individual tiles attached to the hull of a spacecraft. Such protective tiles usually consist of upper and lower shells (plates) between which there is a honeycomb core.

The tiles are mechanically attached to the hull of the spacecraft. At the same time, tiles can be integrated either into a single system or separately from the body with subsequent placement on surfaces requiring thermal protection.

Such integration requires welding or soldering of the plates simultaneously with the installation of a U-shaped flexible heat-compensating element, as well as additional fasteners (legs) that secure the thermal protection elements on the surface of spacecraft (Fig. 1).

The promising materials used to create heat-shielding systems are multicomponent alloys based on (Ni–Cr), in particular, a five-component powder composite material consisting of metallic (Ni–Cr), intermetallic (Al–Ni_3) and oxide (Y_2O_3) phases. However, its application, despite numerous advantages, is difficult due to the exceptional complexity of welding or brazing [3–5] of non-rigid thin structural elements.

So, according to [5], when soldering structures in a vacuum furnace, prolonged exposure to high temperatures leads to the appearance of residual thermal deformations of the processed parts (Fig. 2), causing their warpage. The stability of the strength and density of the weld is

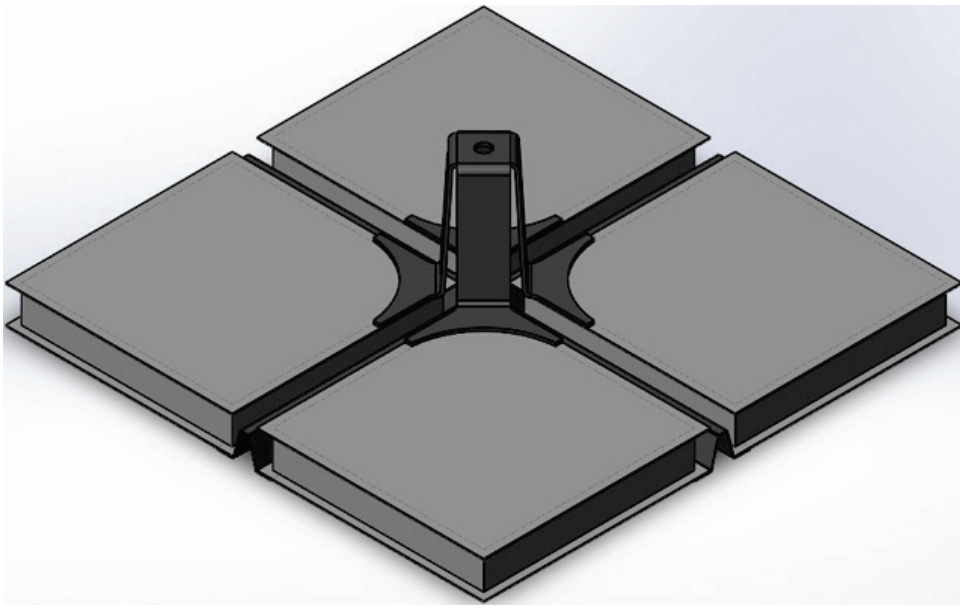

Fig. 1. Typical heat-insulating systems of spacecraft and their design. *1*—top plate; *2*—bottom plate; *3*—honeycomb filler; *4*—side plate.

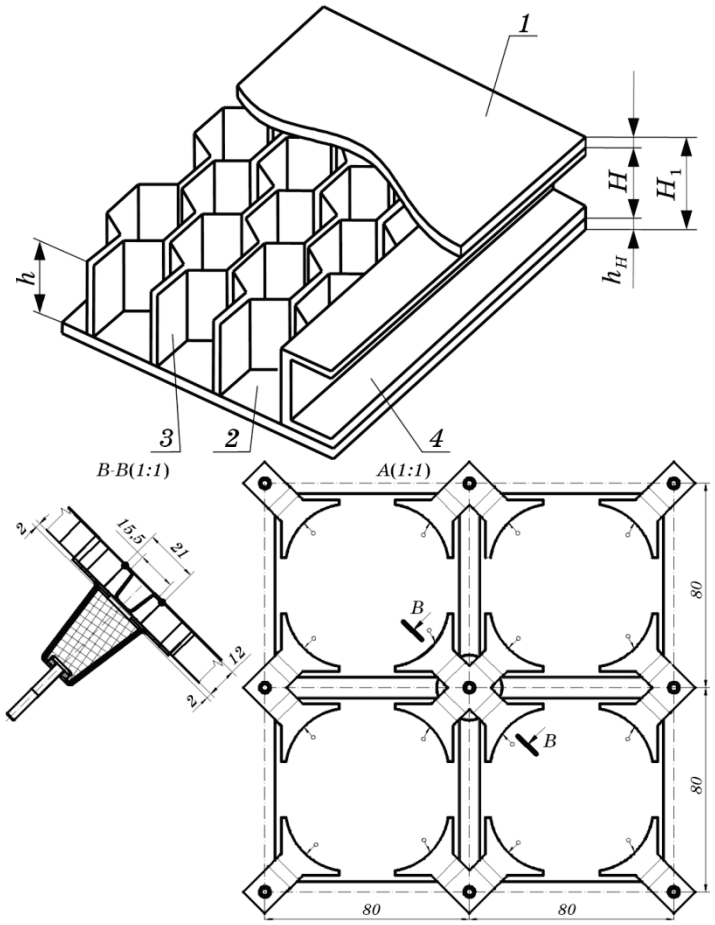

Continuation of Fig 1.

significantly reduced. The recommendation to solder in one installation is only applicable while fixing the top and bottom panels, as well as the U-shaped inserting between these panels.

The efficacy of the lasers system use in welding and related operations (different processing of the surface layer) is considered in several works [6–10]. Is usually the process is that the concentrated flow of energy enters the surface, where it is absorbed with the release of a large amount of heat.

The focused beam of high intensity, capable to evaporate the basic material and to form a steam capillary (lock slit), allows to weld elements and details with deep penetration. By moving the melt zone along the weld area, it is possible to connect thick-walled parts (Fig. 3, *a*), or parts that require significant welding. Typically, the wavelength

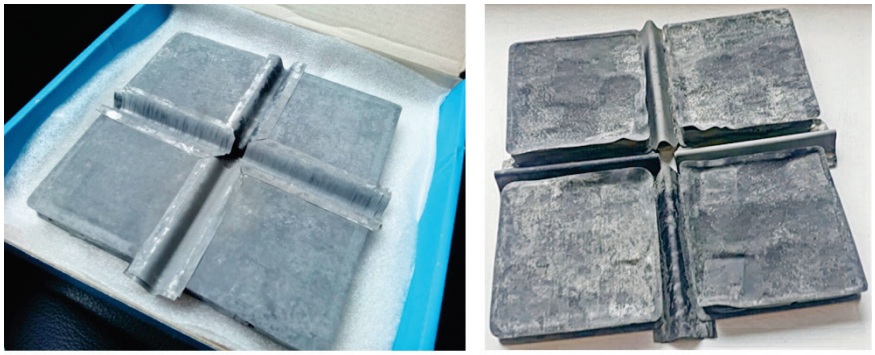

a *b*

Fig. 2. Test body. *a*—initial; *b*—residual thermal deformations of workpieces after fire testing.

of modern laser radiation sources belongs to the near infrared region.

Due to the formation of the steam capillary, the degree of reflection of radiation is reduced to 10% , simultaneously with the increase in the depth of thermal penetration, which allows in some way also to equalize the thermal stresses arising during welding.

Solid-state or gas lasers with a power of 0.5 kW to 20 kW, which usually have fibre-optic means of transporting the beam, are used for welding. Pulsed lasers with lower power are used for precision welding, including refractory metals and alloys.

In [6] the authors analyze in detail the possibilities of using lasers of different types in certain processing technologies, authors of [7] give the comparison of laser and plasma effects on materials for cutting, welding, modification and the like.

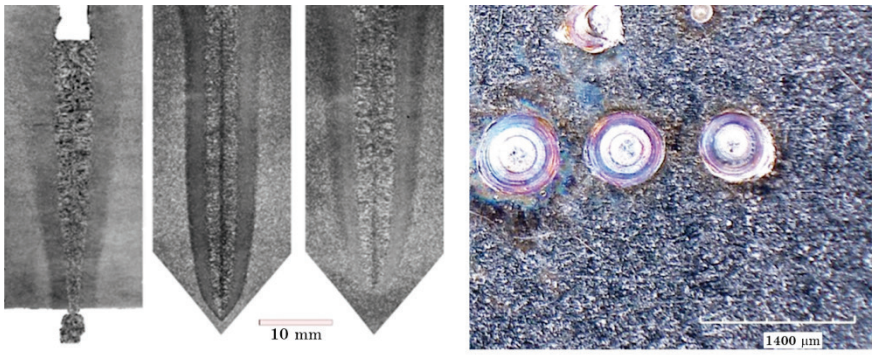

a *b*

Fig. 3. Laser keyhole forming (*a*) and discrete melt bath formed by pulsed laser (*b*) according [12] and [13].

The authors of [8] give the features of using gas lasers for welding non-ferrous metals, alloyed [9], heat-resistant and difficult-to-machine materials [10]. Some researchers believe that a higher quality of permanent joints is provided under conditions of high or low vacuum [11] now. In this case, it is possible to remove various contaminants from the surface, to ensure the cleanliness of the weld pool. The absence of air or gas environment prevents thermochemical processes in the surface layer. This is especially true for cases when joints are made from materials prone to embrittlement and warpage.

Traditionally, laser vacuum welding is used for one-piece connection of critical elements and parts that require stable quality and strength.

Different papers provide information on laser welding of thin sheet blanks [12]. When working in pulse mode, a discrete melt bath is formed (Fig. 3, *b*).

It is known that the main problems of welding Ni-based heat-resistant alloys are put down to the formation of hot cracks in the weld metal and the heat-affected zone [13], as well as a number of crystal lattice defects, which sharply reduce the mechanical properties of the joint and in some cases make fusion welding difficult.

At the same time, the mechanism of initiation and development of cracks has not been sufficiently studied.

It is believed that the nucleation can take place both during the crystallization of the weld pool (crystallization cracks are formed), and during the cooling of the metal and the transition to the solid state (polygonization cracks are formed).

It is certain that the insufficient strength of the weld and its low deformation capacity are associated with the formation of microcracks.

To combat cracks, the purity of the components to be welded is increased and local powerful energy sources (laser, e-beam) are used [14].

Another problem is the porosity and low bond strength rendered by a high sensitivity of Ni to the content of impurities (P, S) and the increase of dissolved gases concentration in the weld metal. 'Hydrogen disease' occurs due to a sharp decrease in the solubility of O_2, H_2, H^+ and CO with a decrease in the temperature of the deposited liquid metal and limited opportunities for gas leakage during the crystallization of the welded joint.

However, the greatest degree of pore formation in Ni-based alloys is associated with nitrogen saturation especially in the presence of oxygen. The weld metal is prone to embrittlement and the formation of a microcracks mesh, which is caused by the appearance of the Ni–NiO eutectic (T_{pl} = 1438°C) distributed outside the crystallites during the cooling of the welding molten bath.

This reduces the strength of the grain boundaries, makes the welding seam not only porous but also brittle.

So, the prospect of using a vacuum chamber to ensure reliable pro-

tection of the welding zone from the atmosphere, as well as the use of high-purity filler metals or laser welding, is reasonable and justified.

It is of interest to weld elements of the heat-resistant dispersion-hardened alloy Ni–20Cr–6Al–Ti–Y_2O_3 by methods of local (high intensity) heating of the contact zone using the laser.

Since the connected panels are thin, it is necessary to provide such conditions for laser welding, which will be free of both through firing and significant residual stresses leading to the formation of microcracks after cooling.

The aim of the work is to study the laws of formation of parameters of strength and reliability of fixed joints from sheet blanks of small thickness from materials based on nickel and chromium.

2. EXPERIMENTAL PROCEDURE

Integration of the elements into a single body is performed by laser welding in vacuum chamber with the use of finely dispersed Ni-based solder and without it. Simultaneously, other high-temperature dispersed alloys are used. To control the weld condition and study the material structure an electron scanning microscope REM-106-I (Ukraine) is used.

To identify the composition and structure of multicomponent alloys by scanning electron microscopy, the thermal etching method is used. The essence of the method is to heat the samples up 550°C, with a holding time of 12 min after obtaining thin sections with a surface roughness of *Ra* 0.16 μm.

Sections are made according to the standard technique, material removal is less than 0.08 mm, and there are no surface defects. The size of the welding zone is changed by means of electromechanical focus control, which made it possible to ensure the local heating of the surface from 0.27 mm to 1.8 mm in diameter. The composition of the elements of the joint zone as well as adjacent areas is studied. The study is carried out by the method of energy dispersive X-ray microanalysis. At the same time, along with the alloy Ni–20Cr–6Al–Ti–Y_2O_3, studies are also carried out on other materials, the mechanical properties of which are given in Table. 1.

Welding in vacuum is carried out using a laser complex LSK-400-5 and a universal vacuum station VUP-5 [15] (Fig. 4). Some technical characteristics of LSK-400-5 are given in Table 2.

While welding, the beam in the plane of the upper workpiece is focused. Positioning is carried out by using a transverse movement table which provides welding at several points with different duration of the process. The duration of the process is from 0.1 to 0.15 s.

The effect on the surface is controlled by a mechanical beam chopper with an electric drive. The chopper is installed in the chamber through

TABLE 1. Based on nichrome mechanical properties of the used alloys.

Characteristic	T, °C	Base YuIPM-1200	Ni20Cr3Al	Ni20Cr6Al reinforced Y_2O_3
Aluminium content,%	–	–	3.0	5.0–6.0
Density, m^3/kg	–	8300	7950	7500
Tensile strength, σ_w, MPa/MPa/kg	20	738/0.09	1020/0.136	1005/0.134
	800	237/0.03	542/0.07	999
	1100	45	–	–
	1200	–	40	56
Yield strength $\sigma_{0.2}$, MPa	20	364	624	760
	800	228	457	687
	1100	40	–	–
	1200	–	35	51
Elongation δ, %	20	36.5	21	12.9
	800	36.7	18.1	2.0
	1100	32.8	18	–
	1200	–	18	22.3

the optical beam transport system. Placement of samples in a vacuum chamber is performed so that the weld bath is formed in the horizontal plane.

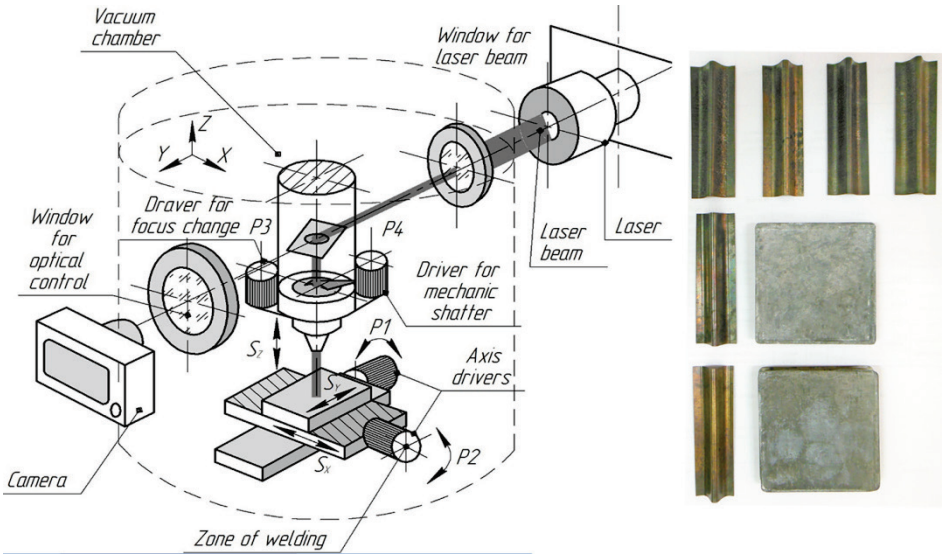

Fig. 4. The equipment used and the scheme of the beam exposure to the surface and parts of workpieces.

TABLE 2. Technical characteristic LSK-400-5.

No.	Characteristic	
1	Hydraulic drive power, kW	40
2	Number of controlled coordinates	5
3	Number of simultaneously controlled coordinates	3
4	Desktop dimensions, mm	500×1000
5	Laser type and beam wavelength, nm	Nd:YAG, 1062
6	The power of the laser average, W	410
7	Pulse frequency, Hz	50–1000
8	Accuracy of movements, mm	±0.05
9	Energy per pulse max, J	600

Welding is carried out both with and without filler metal: 1) quick-setting high-temperature powder solders type of VPR [10] (based by Ni), Table 3; 2) finely dispersed Ni powder (Ni; 5% W; 1.0–1.5% B).

Mechanical tests of the finished specimens are performed on a P-20 tensile testing machine equipped with an m-Daq ADC data acquisition system and means for displaying the load diagram (Fig. 5).

The mock-up heat-shielding section (TZS) consists of four three-layer honeycomb panels 72×72 mm in size. (Fig. 1), and four thermal compensators—U-shaped connecting elements (Fig. 2).

The connecting element consists of a package of two profiled plates with a thickness of 0.15 mm each. The edges of the connecting element and the three-layer panel are butt welded and overlapped, while ensuring a reliable connection. The height of the weld should not exceed 1.0 mm, and its width should be 2.0 mm.

TABLE 3. Quick-setting high-temperature powder solders (from granules) based on Ni.

	Contained, % mass											*T* of use, °C
	C	Cr	Al	Co	Mo	Nb	W	B	Si	Ti	Fe	
VPR11	0.5–0.6	14.0–16.0	0.1–1.01					2.0–3.0 0.6–1.2	4,0–5,0 1.8–2.2	–	3.0–5.0	1050–1120
VPR24	0.1–0.15	6.0–7.0	4.0–5.0	8.5–9.5	1.6–2.0	10.0–11.0	8.5–9.5	0.25–0.35	2.5–3.0	0.3–0.9	–	1210–1225
VPR36	0.15–0.2	8.0–10.0	2.5–6.0	8.0–10.0	1.4–2.0	2.0–5.0	2.0–6.0	0.8–1.1	–	–	–	1250
Finely dispersed Ni powder				0.1–0.2	1.6–2.0							

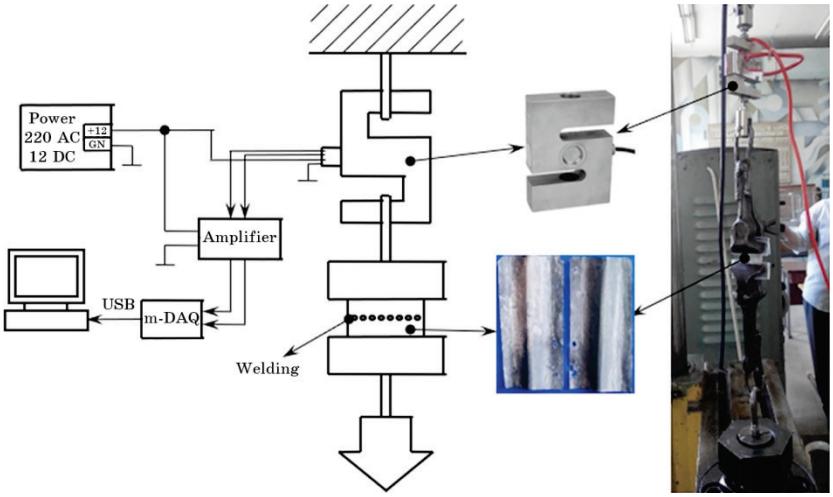

Fig. 5. The equipment used for mechanical characteristic identificating.

Pre-formed elements and details of the panel are used for welding, having performed their metrological verification and surface preparation.

It is taken into account that the formation of a U-shaped element to compensate for thermal deformations did not provide full compliance with the drawing, and the joint surfaces also required grinding to a roughness of *Ra* of 0.32 μm. It is also taken into account that the mechanical properties of heat-resistant alloys significantly depend on operating temperatures.

Based on the alloy properties of Ni–Cr composites given on Table 4. The mechanical properties of the connection should correspond as fully as possible to the properties of the base material.

TABLE 4. Ni–Cr based alloy properties.

	Parameter	Temperature T, °C		
		20–100	700	1100
1	Tensile strength σ_v, MPa	738	237	45
2	Yield strength $\sigma_{0.2}$, MPa	364	228	40
3	The limit of proportionality σ_{nn}, MPa	356	222	39
4	Elongation δ %	36.5	36.7	32.8
5	Relative narrowing ψ, %	34.2	32.6	19.0
6	Density ρ, kg/m^3	8300.0	–	–
7	Thermal conductivity λ, W/(m^2·K)	(10–11)	(28)	–
8	Specific heat C, kJ/(kg·K)	(0.44)	(0.6)	–
9	The degree of blackness of the surface, ε	0.8–0.85	–	–

3. EXPERIMENTAL RESULTS AND DISCUSSION

Some aspects of heat tasks given on the [17], however, the pulse heating model of laser melting requires special conditions.

The pulsed laser operating at fixed frequencies simulation. In the simulation, it is assumed that the heating of the plate surface alternated with the propagation of heat into the material at the moment of the absence of a pulse. Given result of [13], [14], let into account that the distribution of the radiation intensity at the laser exit aperture obeys the Gaussian law:

$$I(w) = I_0 \exp(w^2/w_G^2),$$

where I_0 is the radiation intensity on the beam axis; w—current radius; w_G is the radius at which the radiation intensity decreases by a factor of e. Also based on the well-known uneven heating equation

$$\frac{\partial T}{\partial t} = \alpha\left(\frac{\partial^2 T}{\partial x^2} + \frac{\partial^2 T}{\partial y^2} + \frac{\partial^2 T}{\partial z^2}\right)$$

with boundary conditions on the surface from the action of the source:

$$-k\frac{\partial T}{\partial z}\bigg|_{z=0} = q(x, y, t),$$

where $q = q_0(1 - R)$, q_0 is the radiation power density; R is the surface reflection coefficient; k is the coefficient of thermal conductivity of the material; the z axis is perpendicular to the surface and directed deep into the material. From where the heat distribution is described as follows:

$$T(x, z, t) = \frac{q(x)r^2}{\lambda}\left(\frac{\alpha}{\pi}\right)^{1/2}\int_0^t \frac{P(t-\pi)\exp\left[\frac{z^2}{4at} - \frac{x^2}{4a\tau}\right]}{\sqrt{\tau}(4a\tau + r^2)}d\tau, \quad (1)$$

where λ is the thermal conductivity coefficient; a—thermal diffusion of the material of the workpiece; t is the current time; P—power of laser radiation.

Temperature on the surface of a semi-infinite body at a point with coordinates (x, y, z) provided that the laser beam moves along the surface with a speed υ, and provided that heat losses from the surface are ignored:

$$\overline{T} = \frac{16}{\sqrt{\pi}}\int_0^\infty \frac{1}{\sqrt{(c'^2 + \tau^2)}(b'^2 + \overline{\tau}^2)}\exp\left[-\frac{(2\overline{x}'^2 + \overline{\upsilon}'\tau)}{4(\overline{c}'^2 + \overline{\tau}^2)} - \frac{\overline{y}^2}{\overline{b}^2 + \overline{t}^2} - \frac{\overline{z}^2}{\overline{t}^2}\right]d\tau, \quad (2)$$

where $\bar{T} = \dfrac{16\sqrt{\pi K r T}}{P A_0}$; $\bar{\upsilon} = \dfrac{\upsilon_r}{2a}$; $\bar{x}' = \dfrac{x}{r}$; $\bar{y}' = \dfrac{y}{r}$; $\bar{z}' = \dfrac{z}{r}$; $\bar{c}' = \dfrac{c}{r}$; $\bar{b}' = \dfrac{b}{r}$; $r^2 = cb$; A_0—reflectivity of the workpiece material; P—power of laser radiation; b, c—parameters of the laser density distribution.

In this case, the temperature change is determined:

$$T(x,z,t) = \frac{P}{\pi \dfrac{1}{2}\rho c}\int_0^t \frac{e^{\frac{(x-\upsilon(t-z))^2}{4\alpha\tau+A^2}\frac{y^2}{4\alpha\tau+B^2}}}{\left[(4\alpha\tau+A^2)(4\alpha\tau+B^2)\alpha\tau\right]^{1/2}} \times \\ \times\left[e^{-\frac{z^2}{4\alpha\tau}} - \eta(\pi\alpha\tau)^{1/2}\operatorname{erfc}\left(\frac{z}{2(\alpha\tau)^{1/2}} + \eta(\alpha\tau)^{1/2}\right)e^{\eta z+\eta^2\alpha\tau}\right]d\tau, \tag{3}$$

where x, y, z are coordinates; t is time; η is coefficient of heat transfer from the surface of the workpiece; α is the thermal conductivity coefficient; A and B are major and minor axes of the heating spot; $P = \pi qAB$ is the power of the emitter. The heat distribution will occur in the plane of the limited thickness plates.

At the end of the period between laser pulses, the surface temperature is determined by

$$T(t) = T\frac{q_l\delta}{\lambda}\left[\frac{2}{\sqrt{\pi}}\frac{\sqrt{a(t-\tau)}}{\delta} + \exp\left(\frac{a(t-\tau)}{\delta^2}\right)\operatorname{erfc}\left(\frac{\sqrt{a(t-\tau)}}{\delta}\right)\right]_{\max}, \tag{4}$$

where δ is the depth of heating; $q_l = f(f^c, p, t)$.

Under the conditions of pulsed laser exposure, the theory of thermal destruction is usually used to describe the evaporation mechanism.

The one-dimensional problem of thermal conductivity in the coordinate system associated with a moving boundary, with the evaporation of a semi-infinite body, has the form

$$\left.\begin{aligned} &\frac{\partial T}{\partial T} = \upsilon\frac{\partial T}{\partial z} + a\frac{\partial^2 T}{\partial z^2} \\ &-K\frac{\partial T}{\partial z} = q\upsilon - \rho\upsilon\Delta H, \quad z = 0 \\ &T(z,0) = T(\infty,t) = 0 \end{aligned}\right\}.$$

where υ—the velocity of the evaporation front; ΔH—the difference between the specific enthalpies of the solid and gaseous phases:

$$\Delta H = L_U - \frac{1}{2}R_0 T,$$

L_U—specific heat of vaporization; R_0—universal gas constant.

Let the process is stationary, so the solution of the boundary value problem in a moving coordinate system has the form

$$T(z, t) = T_0 e^{-\frac{z\upsilon_0}{a}} = \frac{q - \rho\upsilon\Delta H}{\upsilon c\rho} e^{-\frac{z\upsilon_0}{a}}, \tag{5}$$

here

$$\upsilon_0 = \frac{q}{\rho\left(L_U + 2.5\dfrac{R_0 T_0}{A}\right)}.$$

In the conditions of intensive evaporation after some time from the beginning of influence of laser radiation (delay time t_U) the constant speed of movement of the evaporation front in depth of material ν_0 is established.

The delay time is determined by the equation as

$$t_U = \frac{\pi K\rho c(T_U - T_0)}{Uq^2}, \tag{6}$$

where C—specific heat; T—intense evaporation temperature; T_0—initial temperature.

Consider the distribution of heat in the body, provided that the radiation power is evenly distributed on some treated surface, and the radiation arrives normally. In time δt the energy $W\delta t$ will reach the surface. The volume of evaporated material will be for the formed funnel Sbl. Based on the law of conserved energy we have the equation: $Sh\rho bl = W\delta t$, where h—the amount of heat required to evaporate a unit mass of material; ρ—material density.

Transforming this expression and assuming that we will have the growth rate of the funnel as:

$$\frac{ds}{dt} = \frac{W}{h\rho\rho s}. \tag{7}$$

On the other hand, there is a certain transfer of energy deep into the material due to thermal conductivity. This phenomenon leads to the formation of a destructive layer—a layer with altered physical and mechanical properties. The problem of the motion of the phase boundaries taking into account the thermal conductivity is known as the Stefan problem. Assuming that the heat spreads normally to the surface, we have a one-dimensional non-stationary equation of thermal conductivity as

$$\frac{\partial^2 T}{\partial z^2} = \frac{1}{D}\frac{\partial T}{\partial t} \tag{8}$$

for the temperature inside the material $T(z,\ t)$ together with the boundary conditions at the moving border $z = l(t)$ and on the reverse side of the workpiece. So, $D = K/(\rho c)$—temperature conductivity; K, ρ, c—thermal conductivity, density and specific heat.

The condition on the moving boundary is obtained as a result of using the law of conservation of energy in the form as

$$\frac{W}{A} = L_v \rho \frac{ds}{dt} - K \frac{\partial T}{\partial z}, \tag{9}$$

where L_v—latent heat of vaporization per unit mass.

Another limiting condition is that the temperature of the moving limit is approximately equal to the temperature of the boiling point, so and $z = l(t)$, $T = 0$, when $l \to \infty$.

Despite the fact that in practice there is some evaporation of the material at the boiling point, the approximation is satisfactory.

While maintaining sufficient accuracy, it is possible not to take into account the violation of continuity at the phase boundary.

This formulation of the problem is more difficult than the classical one, but obtaining a simple solution is possible when the velocity of the boundary moves close to the velocity in the limit mode of evaporation. Then there will be equation as

$$\left| \frac{K(\partial T/\partial t)l^*}{L_v \rho (dl/dt)} \right| = \frac{KO(T_v/l^*)}{L_v \rho O(W/h\rho A)}, \tag{10}$$

where the characteristic distance at which the temperature drops in the material. This distance is

$$l^* = \frac{D}{(W/h\rho A)}. \tag{11}$$

Then for dimensionless velocity of the evaporation limit depending on the dimensionless time

$$\frac{d\xi}{d\tau} = \left[1 + \varepsilon \left\{ \frac{1}{2} \operatorname{erfc}\left(\frac{\tau^{1/2}}{2} \right) - \frac{1}{\pi\pi\tau^{1/2}} e^{-\frac{\tau}{4}} \right\} \right] \times$$
$$\times \frac{2}{\pi} \left\{ 1 + \frac{\varepsilon}{\pi\tau^{1/2}} \right\} \arcsin \left\{ \left(1 - \frac{\pi\varepsilon^2}{4\tau} \right)^{1/2} \right\}. \tag{12}$$

Solving this equation allows us to calculate the growth dynamics of the molten bath during the time of laser exposure to a certain area of the surface. Together with (12) it is possible to estimate the shape of the groove after exposure to a pulsed laser beam and to determine the

dynamics of the destruction of the material, *i.e.* to determine the thickness of the layer with altered physical and mechanical properties.

In this case, it is taken into account that plates of shallow thickness are in contact with each other along a limited plane. The deformation of the plates and loose contact are not taken into account.

The problem is solved for two cases: 1) contact welding of plates along the plane; 2) butt welding in the wall area.

The curves of semi-obtained temperature increase on the surface and over the cross section are shown in Fig. 6. Table 5 also shows the results of modelling the process for the cases of contact welding and butt welding, implemented in ANSYS [15]. To control the temperature used the probe: 1st—on the centre of welding point; 2nd—on the upper panel. The patterns of temperature distribution over the surface and over the section of the workpieces in the contact zone are obtained. The time (number of pulses) has been determined for the temperature in the centre of irradiation to reach 1475°C (temperature of phase transformations) and 1800°C.

Thus, the zone of formation of hot microcracks can be significant and have the area up to 2–3 areas of laser action. Uneven heating, as follows from Table 5, will lead to the formation of localized macrodefects, including intermetallics, which reduce the strength of the joint. For Nd:YAG laser when operating at a frequency of 125 Hz with a power of 0.5 kW, the heating time of the welding point of 0.8 mm part should not exceed 40–45 ms.

After laser exposure, temporary destruction in the area of exposure is possible, with the formation of burn-through (holes) at the point of contact of parts, as shown in Fig. 6, *a*.

Preliminary heat treatment is carried out while preparing samples for welding (forming U-shaped elements, honeycomb filler strips).

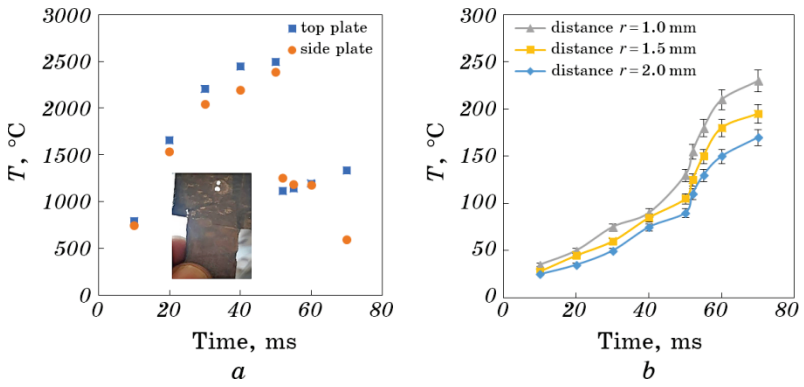

Fig. 6. Temperature rise in the heating centre (*a*) and behind the area of direct irradiation (*b*).

This made it possible to improve the structure of the processed ele-

TABLE 5. Results of modelling the vacuum welding process.

Welding options and modes	Scheme and the distribution of heat on the surface of the workpieces	Temperature fields
Contact Thickness: $\delta_1 = 0.14$ mm; $\delta_2 = 0.14$ mm; $d_0 = 0.5$ mm; $H = 14.0$ mm; clamping force—5 N; beam power—400 W; pulse repetition rate—125 Hz; pulse energy—8 J. 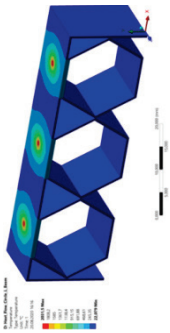	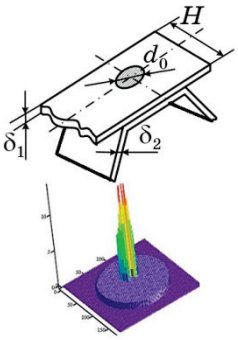	1st probe—on central point 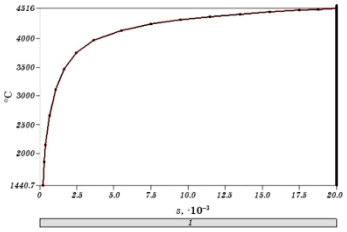 2nd probe—on upper panel 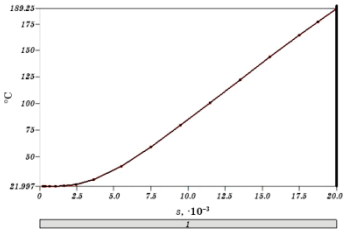
Edge Thickness: $\delta_1 = 0.14$ mm; $\delta_2 = 0.14$ mm; $d_0 = 2.5$ mm; $H = = 14.0$ mm; clamping force—20 N; beam axis angle—$\pi/4$ (coordinate system XOZ_1Y_1); beam power—400 W; pulse repetition rate—125 Hz; pulse energy—8 J. 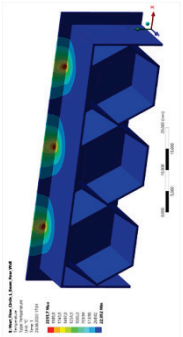	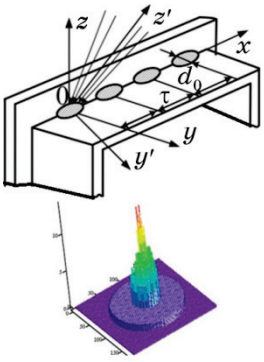	1st probe—on central point 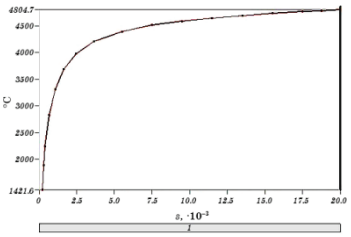 2nd probe—on upper panel 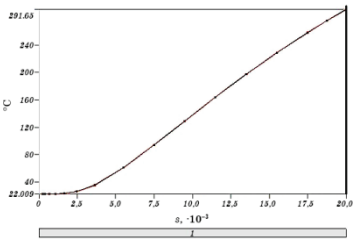

ments and to reduce the interlayer cracking of the material with the release of some particles of coagulated material used in sintering (Fig. 7, *a*, *b*; Fig. 8).

The workpieces are destroyed even with relatively small deformations without heat treatment. Based on the results of modelling temperature fields (Table 2) according to (4), the welding mode is selected.

Microelectronic analysis of the welding points showed that the weld bath is formed unevenly; the material splashed out of the weld pool and formed a rather large (up to 200 μm) droplet influx. Almost all points had through penetration (due to the shallow thickness of the workpieces, $h = 0.14–0.4$ mm), while the shape of the obtained holes differed from the correct geometric circle. This is due to the fact that the used laser with a wavelength of 1062 nm with the specified pulse generation parameters is powerful enough to perform welding operations. The attempt to form a seam with a linear feed motion slightly improved the results, however, it is not possible to fully obtain stable seam parameters. The reason may also be the shutter used the response time of which ($T = 0.07$ s) is comparable to the duration of the laser action on the surface. The model of the heat-shielding element and the microe-

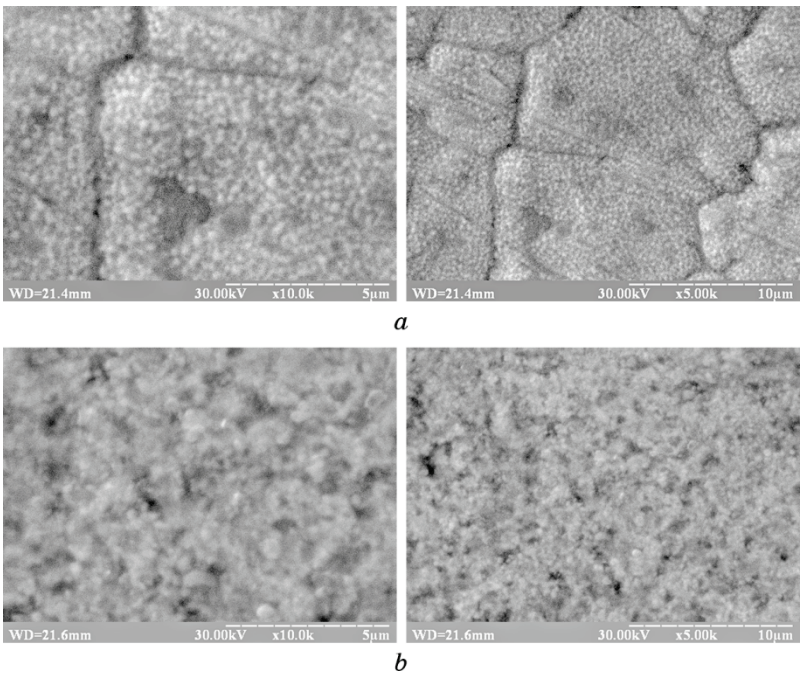

Fig. 7. Breaking of the workpiece (0.4 mm) during bending. *a*—before heat treatment; *b*—after heat treatment.

lectronic photo of the welding places are shown in Fig. 8.

It is found out that the low thermal conductivity of nickel and nickel alloys during welding leads to the increase in grain size and, as a consequence, to a decrease in the toughness and strength of the weld in general.

The attempts to carry out the heat treatment aimed at preventing structural changes in the welding zone and in the near-welding zone are less effective than the introduction of melt modifier additives (Ti, Mo, Al) and limiting the welding energy per unit length.

Prevention of the formation of nickel aluminides is carried out by rapid cooling the samples for 3 to 5 min after welding by blowing a vacuum chamber with argon cooled to a temperature of –30…–20°C.

The analysis of the welding points (Fig. 8) showed that the weld pool is not formed uniformly, with the material splashing out of the weld pool and the formation of rather large (up to 200 μm) drip sag.

Almost all the points had through penetration (which is caused by the shallow thickness of the workpieces, h = 0.14…0.4 mm), while the shape of the obtained holes is different from the geometric regular circle. Comparison with the theoretical parameters of the weld pool showed that the actual dimensions of the melting point are significantly larger than the theoretical ones, Fig. 9, and the deviation from the

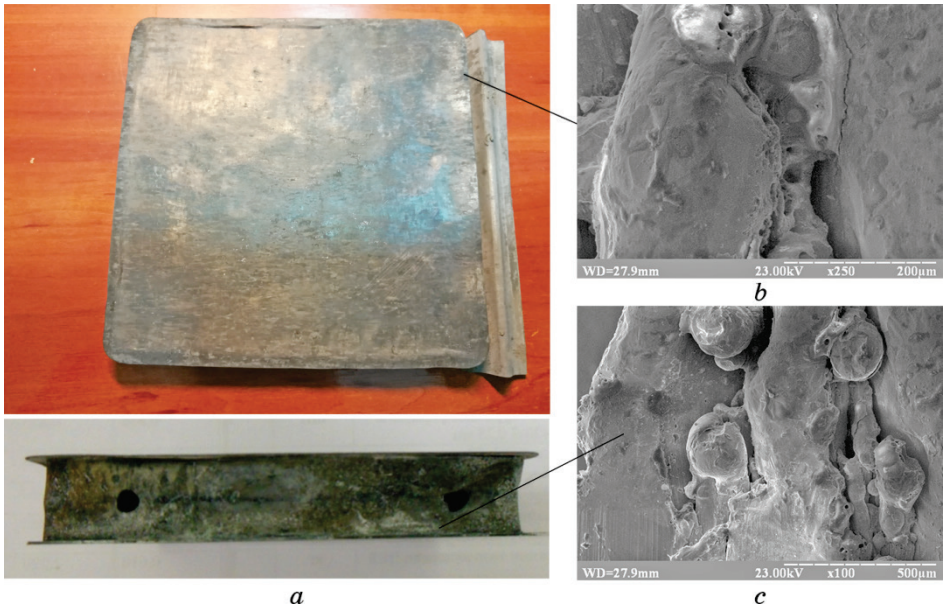

Fig. 8. Real model of a heat-shielding panel made of alloy Ni–20Cr–6Al–1Ti–1Y_2O_3 (*a*) and microelectronic photos of elements of the weld bath (upper side (*b*) and down side (*c*)).

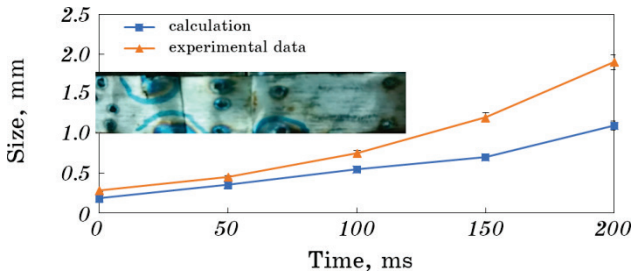

Fig. 9. Comparison of the sizes, mm, of welding points depending on the time, ms, of exposure to the beam.

correct shape indicates that the melting of the material occurs rather unevenly.

The microelectronic images obtained by us when studying the ends of the bath confirm the same thing. This situation can be explained by the fact that the used infrared laser with a power of 500 W with the indicated pulse generation parameters is powerful enough to perform welding operations, and the formation of the seam should occur with a linear feed move.

The cause may also be the shutter used the response time of which is comparable with the duration of the exposure.

The result of studying the trace element composition of the welding zone with and without filler metal (Fig. 10, *a*) is also of our interest. The analysis is carried out at three points—directly in the melt zone, in the near region of the weld, which is heated above 950°C, and on the supporting surface (Fig. 8, *b*).

Table 6 shows a comparison of the results obtained laser welding and brazing in vacuum (both in a clean zone and using a filler powder of the VPR type).

The presence of a significant proportion of C is caused by carbon

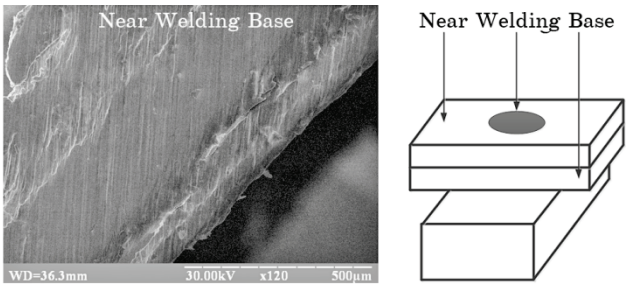

Fig. 10. Study of an element of the weld zone on a thin plate. *a*—microelectronic photograph of the welding zones; *b*—diagram of welding zones.

'poisoning' of the surface from the graphite tile of the Table 6, which is used as a thermal insulation element together with ceramic plates of Al_2O_3. This becomes obvious if we neglect the insignificant proportion of Na, S, Cl, K, Ca detected during the analysis and present in parts of the vacuum chamber.

The presence of oxygen at the points under study can be explained by the oxidation of a rather loose layer on the surfaces (Fig. 10), and this oxygen remains in the molten bath after the process is finished. It is obvious that the use of laser welding provides better structural and elemental characteristics, since the lack of atmosphere and local heating do not lead to significant changes in the base material in the area around the weld.

The use of solders as filler materials has a definite effect on the structure and quality of the formed weld; however, it requires further optimization of the process.

In this case, only partial melting of one of the plates is possible, and when using additional heat conductors and ballasts, the process can be reduced to a process [11].

Subsequent mechanical tests of the resulting joint showed that the welded joint is destroyed by a static load perpendicular to the plane of formation of the weld point. It is found that the fault occurs mainly in the heat-affected zone, in the place of cracking.

At the same time, it is noted that a significant decrease in the number of pulses (up to 5–10 per cycle) leads to the formation of a low-strength joint, although no burn-through of the weld is observed.

Due to local heating of the workpiece, no significant structural

TABLE 6. Mass fraction of elements for various types of welding.

	Laser welding			Laser welding with VPR (air plasma cutting)			Soldering process		
	Near	Welding	Support	Near	Welding	Support	Near	Welding	Support
C	24.3	15.81	4.79	33.8	12.1	4.79	57.25	52.16	7.75
O	4.6	3.05	6.67	4.6	17.4	16.7	34.96	34.96	2.51
Na	2.38	0.07	0.23	2.4	–	–	–	–	–
Al	2.76	5.72	6.63	1.7	22.1	16.6	–	–	6.16
S	0.28	0.05	0.0	–	–	–	–	–	–
Cl	2.25	0.0	0.04	–	–	–	–	–	–
K	0.47	0.08	0.01	–	0.2	–	1.15	2.93	–
Ca	0.39	0.1	0.1	–	–	–	0.48	0.47	–
Ti	0.56	0.1	0.0	–	1.18	–	1.1	1.31	–
Cr	17.6	15.8	21.6	10.7	6.15	20.7	1.15	9.95	17.55
Ni	44.2	58.1	59.04	43.8	37.2	39.2	0.45	–	64.33
Y	0.21	1.12	0.89	0.4	0.8	1.9	1.1	0.2	1.9

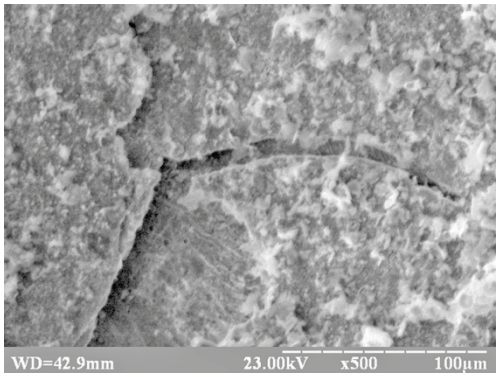

Fig. 11. Grids of microcracks in a weld at insignificant dynamic loading.

changes are observed. At the same time, the resulting joint is prone to cracking with destruction of the contact zone when the load of 30–40% of the critical value for the material is applied (Fig. 11).

Comparison of the results of welding without filler metals and solder for VPR showed that the spread of adhesion strength at five points on ten samples is higher, when are welded with additives. At the same time, the strength characteristics continue rise slightly. Another important characteristic is elongation, which is the maximum for welding with filler material. It accounts for only 30–35% of the characteristics of the starting material (Fig. 12).

Further development of the process can improve these indicators, most likely by preventing the formation of a porous structure with microcracks. Since the initial billet from Ni–20Cr–6Al–Ti–Y_2O_3 obtained by powder metallurgy [16], is subsequently rolled into sheets of the required thickness (0.4–0.14 mm), changes in its structure and phases

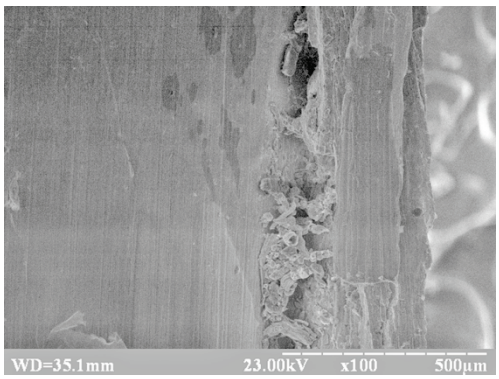

Fig. 12. The appearance of a porous structure at the welding site when using additive materials.

occur. At the same time, the initial porosity decreases with a simultaneous increase in the number of intermetallic compounds and oxides on the surface. This phenomenon worsens and in some cases almost completely excludes weldability.

Electron microscopic studies have shown that in the Ni–20Cr–6Al–Ti–Y_2O_3 plates there is a clearly pronounced granular structure, and the surfaces of the two mating samples are practically identical. In Fig. 13 the particles are on the order of 1–2 μm; microvoids and cavities are observed in the surface layer. The entire investigated surface (Fig. 13, *b*, *c*) is covered with a network of microcracks.

It can be assumed that the alloy contains a large amount of nickel aluminides, intermetallic compounds with an ordered cubic body-centred crystal lattice. We are able to examine these intermetallic compounds in some micrographs of the end parts of the plates. This explains a number of failures while obtaining a reliable weld joint in the traditional way. The conclusions are also proved by the pictures of the destruction of the samples during mechanical tests on the rupture machine R-20 (Fig. 14). We have that in all cases there is almost fragile destruction of welded points; relative elongation is almost absent.

The presence of additive material has a certain positive effect: the relative elongation of the samples is larger (laser + s), as evidenced by a small horizontal part of the diagram 'stress-deformation', Fig. 14. The tests are performed at a temperature of T = 20°C and at an operating temperature of 600°C (condition of the outer shell of the apparatus at the entrance to the dense layers of the atmosphere).

At room temperature (20°C) obtained quite high values of welding strength: the average yield strength of 350 MPa, but the elongation is less than $\delta < 1\%$. When the temperature rises to 600°C, the results are different: the maximum strength of the weld section in terms of the contact area is 0.4–0.5 of the strength of the base metal or about 130–145 MPa [σ_b], relative elongation of specimens welded with filler material is δ = 1.3...2.2%, without additives—δ = 0.5...1.1%

Since the sintered dispersion-strengthened composite is prone to the

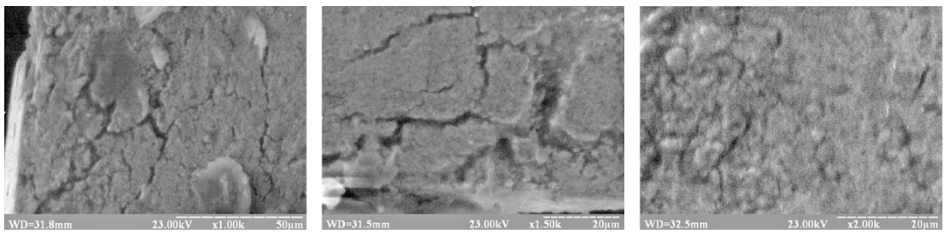

a *b* *c*

Fig. 13. Microphoto of test samples: *a*—surface layer; *b*, *c*—end side of the workpiece 0.14 mm thick.

formation of intermetallic inclusions which affect the mechanical properties of the material, further search for special methods of ensuring the welding process is required.

Another factor affecting the low weldability of elements into a single structure is the unevenness of the structural composition and oxide inclusions observed on the surface of the workpiece, apparently representing conglomerates of Y_2O_3. Rather large areas can be explained by incomplete mix of nanoparticles and their tendency to form separate surface clusters. In these zones, thermodynamic instability can manifest itself, and when exposed to heat they cause an exothermic reaction of aluminium oxidation, as a result of which burn-through and fistulas occur (for thin-sheet blanks).

Thus, improvement of the quality of welding and ensuring the strength of the welded seam is possible both due to more efficient preparation of the initial blanks, and to the optimization of the modes of performing welding in a vacuum chamber [17–19].

Another important point is to ensure a certain temperature regime of welding under which the growth of hot microcracks in the seam and the active formation of intermetallics in the near-weld zone are inhibited.

The use of volumetric heating means simultaneously with laser welding can be an interesting solution to this problem.

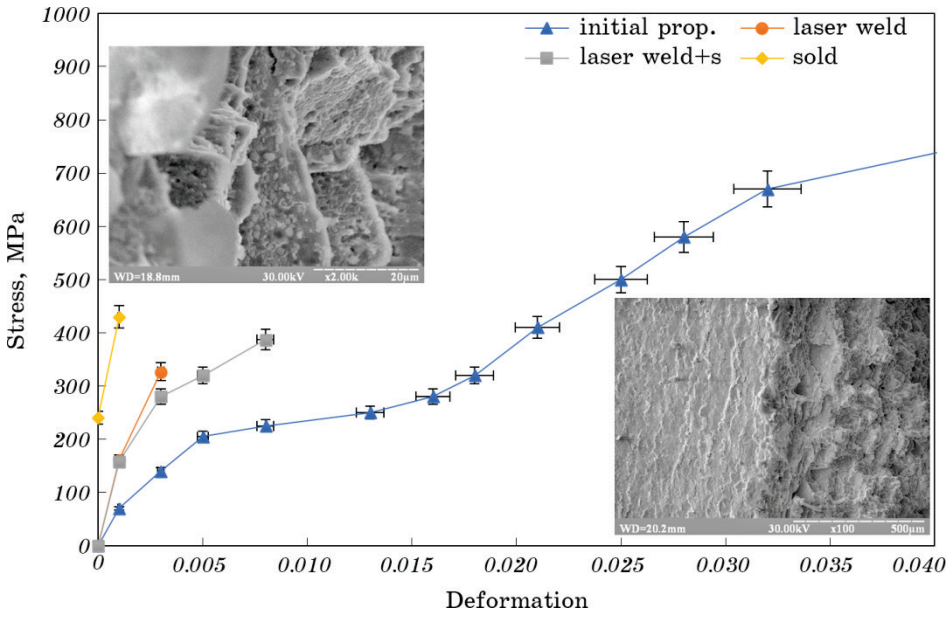

Fig. 14. Results of mechanical tests and fracture of a destroyed specimen obtained under static loading with photomicrographs of destruction of samples under the action of static load.

Taking into account the provisions on the prevention of cracking of the welded seam, further research should be aimed at ensuring a tight fit and high-quality connection of elements before welding. Another way to improve the quality of the joint is to increase the vacuum level to 10^{-3} Pa, as well as to ensure the required cooling cycle of the workpiece. A promising method is a high-frequency laser welding using screens and heat sink elements.

4. CONCLUSIONS

The tests of welded joints made by spot welding of powder dispersion-hardened alloy are carried out.

Welding points made in a vacuum chamber with a pressure of 10^{-2} Pa have burn-through in the weld seam caused by the action of a laser beam, and the diameter of the obtained holes is directly determined by the number of radiation pulses.

A decrease in the number of pulses decreases the strength of the joint point and the maximum strength of the weld section in terms of the contact area is 0.4–0.5 of the strength of the base metal or about 130–145 MPa [σ_b] (the result of testing on the temperature $T = 600$°C).

To obtain a high-quality welded joint, it is necessary to accurately provide the pulse energy and use lasers with a short pulse duration from 1.0 to 50 ms. The laser used did not allow to obtain rational welding conditions, which explains the presence of significant defects and burns at the joints.

It is shown that the presence of special additives in the molten bath (VPR-36 solder is used in the experiments) reduces the change in the parameters of the formed welded joint, while the strength properties of the contact point remain practically unchanged. At the same time, it is due to the introduction of additive material (VPR type) that the relative elongation of the samples is increased to $d = 1.3...2.2\%$.

Further research should be aimed at finding rational welding conditions, ensuring the required composition of the filler metal in the molten bath, as well as the formation of a continuous weld.

Improvements are also required in the vacuum chamber: the use of a drive system for controlled movement of the workpiece will enable more stable welding process.

ACKNOWLEDGMENTS

The work is carried out under the project No. 607182 of the 7th European Framework Program for the creation of ultra-light thermal protection structures.

The authors are grateful for the opportunity to carry out the re-

search data in conjunction with the Yuzhnoye State Enterprise Design Bureau (topic No. 384/17 'Manufacturing and welding of elements of the TZS model'). 'Yuzhnoye' is a high-tech research and production centre of Ukraine in the field of creation and production of spacecraft and launch vehicles, and for which these studies are relevant and significant. Special thanks to the Institute for Problems of Materials Science named after I. N. Frantsevich of the National Academy of Sciences of Ukraine which provided blanks, materials and powders for experimental research. We would also like to express our gratitude to the V. N. Bakul Institute for Superhard Materials for assistance in carrying out certain laboratory studies and tests.

REFERENCES

1. I. O. Husarova, O. M. Potapov, T. A. Manko, Y. V. Falchenko, L. V. Petrushintsev, G. A. Frolov, and V. P. Soltsev, *Tekhnologicheskie Sistemy*, No. 4: 47 (2017) (in Russian).
2. O. Uyanna and H. Najafi, *Acta Astronautica*, No. 176: 341 (2020).
3. V. I. Lukin, V. S. Rylnikov, A. N. Afanasyev-Khodykin, and O. B. Timofeyeva, Welding International, No. 28 (7): 562 (2014).
4. R. Rai, J. W. Elmer, T. A. Palmer, and T. Debroy, *J. Physics D: Appl. Phys.*, No. 40 (18): 5753 (2020).
5. O. F. Salenko, V. T. Shchetynin, Ye. Ye. Lashko, I. O. Husarova, V. P. Solntsev, and O. O. Sytnyk, *Physicochemical Mechanics of Materials*, No. 2: 115 (2018) (in Ukrainian).
6. G. Muthukumaran and P. Dinesh Babu, *J. Brazilian Society Mech. Sci. Engineering*, No. 43: 103 (2021).
7. Ivan Michalec and Milan Marônek, *Acta Polytechnica Hungarica*, No. 9 (20): 197 (2012).
8. C. Cai, H. Chen, and W. Zhang, *Opto-Electronic Engineering*, No. 44 (10): 945 (2017) (in Chinese).
9. I. N. Nawi, M. Saktioto Fadhali, M. S. Hussain, J. Ali, and P. P. Yupapin, *Proc. Engineering*, No. 8: 374 (2011).
10. Y. Geng, M. Akbari, A. Karimipour, A. Karimi, A. Soleimani, and M. Afrand, *Infrared Phys. Technol.*, No. 103: 1 (2019).
11. U. Reisgen, S. Olschok, S. Jakobs, and C. Turner, *Welding in the World*, No. 60: 403 (2016).
12. J. A. Francis, N. Holtum, S. Olschok, M. J. Roy, A. N. Vasileiou, S. Jakobs, U. Reisgen, and M. C. Smith, *J. Mater. Processing Technol.*, **274**: 116269 (2019).
13. Piotr Sęk, *Open Engineering*, **10**, No. 1: 674 (2020).
14. L. I. Sorokin, *Svarochnoe Proizvodstvo*, No. 9: 3 (2004) (in Russian).
15. V. M. Bychkov, A. S. Selivanov, A. Yu. Medvedev, A. V. Supov, B. O. Bolshakov, R. R. Grin, and F. F. Musin, *Vestnik UGATU*, **16**, No. 7: 112 (2012) (in Russian).
16. W. Alnusirat, *Lasers in Manufacturing and Materials Processing*, **6**, Iss. 3: 263 (2019).

17. W. Alnusirat, A. Salenko, O. Chencheva, S. Shlyk, I. Gusarova, and A. Potapov, *EUREKA: Phys. Engineering*, No. 5: 88 (2021).
18. V. Dragobetskii, V. Zagirnyak, S. Shlyk, A. Shapoval, and O. Naumova, *Przegląd Elektrotechniczny*, No. 95 (5): 39 (2019) (in Polish).
19. S. P. Murzin, E. L. Osetrov, and A. M. Nikiforov, *Izvestiya Samarskogo Nauchnogo Tsentra Rossiyskoy Akademii Nauk*, No. 10 (3): 884 (2008) (in Russian).